JOURNAL OF GUIDANCE, CONTROL, AND DYNAMICS
Vol. 29, No. 4, July–August 2006

Spin Axis Attitude Determination Accuracy Model in Presence of Biases

Jozef C. van der Ha*
Mission Design and Operations, Columbia, Maryland 21044

A practical model is presented for the effects of biases on the spin axis attitude pointing orientation of a spin-stabilized spacecraft. Biases are induced by spacecraft design limitations, for example, dynamic imbalance and sensor mounting alignment errors, and by environmental effects such as the variations in the infrared Earth radius seen by the Earth sensor. The measurement equations for the sun and Earth sensors are formulated in the presence of the relevant biases. The effects of the biases on the angular measurements are established by means of a small-angle perturbation technique. The propagation of the biases into the resulting attitude solution is derived by means of a realistic single-frame attitude-determination method. The statistical properties of the expected attitude error can then be expressed in terms of the specified input biases. Furthermore, practical approaches for the reconstruction of the biases from the observed measurement residuals are provided. The models are demonstrated using actual sensor data of the Comet Nucleus Tour (CONTOUR) spacecraft collected during its phasing orbits in August 2002. The sensitivities of the sun and Earth sensor measurements and the attitude vector to the relevant biases are analyzed in detail, and the reconstruction of the biases in the infrared Earth radii is illustrated for CONTOUR's final sensor coverage interval.

I. Introduction

SPIN stabilization represents a convenient and robust spacecraft design concept for many space mission applications. This concept is often used to provide stability during an injection maneuver performed by means of a solid rocket motor (SRM), for instance, when inserting a geostationary spacecraft from a transfer orbit into its geostationary orbit. Spin stabilization may also be used for the injection of deep-space probes into their heliocentric trajectories, as was done in the case of the Comet Nucleus Tour (CONTOUR) mission in August 2002 (Farquhar and Dunham[1]). In any case, it is crucial that the attitude-determination error at the time of the SRM injection is as small as possible; typical requirements for the attitude half-cone pointing error are 0.5 or 0.75 deg. An attitude-pointing error at the time of the injection leads to an error in the achieved orbit, which usually must be corrected afterward by thrusters using onboard propellant. Thus, the attitude error may have a direct impact on the mission lifetime because propellant savings can be used for extending the lifetime of a geostationary satellite[2] or for widening the objectives of a deep-space mission, for instance, by performing another comet flyby.

A typical sensor that is used for the purpose of spin axis attitude determination is the integrated Earth sun sensor of Galileo Avionica. This sensor generates measurements of the sun aspect angle, the Earth chord-length angle, and the sun-Earth dihedral angle, that is, the angle between the plane formed by the spin axis and the sun vector and the plane defined by the spin axis and the Earth vector. The latter two angles are usually measured independently by two infrared pencil beams (with different mounting angles) scanning the Earth's disk.[3]

There exists a large body of literature dealing with the determination of the attitude pointing of a spinning spacecraft, for example, Wertz.[4] When the accuracy of the solution resulting from the attitude-determination process is assessed, it is crucial to distinguish between random and systematic errors. The effects of random errors can be reduced by simply increasing the number of measurements that are used in the estimator (to the extent that the spacecraft attitude remains stable during the interval under consideration). On the other hand, the adverse influences of biases, that is systematic errors, can not be mitigated in a simple manner. Thus, the accuracy of an attitude solution resulting from any method (no matter how sophisticated) may well be contaminated by the presence of significant but unknown bias effects. Sometimes[5] biases reveal themselves when sensor measurements are collected at different times under different geometrical conditions. A quantitative reconstruction or estimation of individual sensor biases is never a straightforward exercise and should be designed and tested with care before its operational use.

An earlier paper[2] contained a covariance analysis for the attitude-determination accuracy in geostationary transfer orbits on the basis of expected bias errors in the sensor measurements. That model provides a useful design tool for optimizing sensor settings and for understanding the evolution of the achievable attitude-determination accuracy over the sensor coverage interval. Furthermore, a single-frame attitude-determination method indicates that a pointing accuracy of less than 1 deg can be achieved in practice under worst-case bias effects. Palimaka et al.[6] provide further insights into the achievable attitude-determination accuracy on the basis of a least-square attitude-determination method. Analyzing data from a number of satellites, they conclude that a worst-case attitude-determination accuracy of 0.5 deg is achievable for the injection of geostationary spacecraft. Sullivan et al.[7] provide useful insights obtained by simulating a number of different attitude-determination methods including estimation procedures for the biases in the Earth chord width and the sun–Earth dihedral angle.

In a previous paper by the author,[8] a straightforward and robust attitude-determination method, that is, the equal-chord method, was presented. It uses angular measurements that are referred to a single point during the Earth sensor coverage interval, namely, where the chords produced by the two pencil beams are identical. The resulting attitude solution is practically insensitive to uniform biases in the measured chord lengths at the time of equal chords.

In the present paper, a fresh look is taken at the nature of the biases affecting the sensor measurements and their effects on the achievable attitude-determination accuracy. Sensor-internal mechanical misalignments and electronic processing biases can be significantly reduced by the careful calibrations of the sensor outputs during prelaunch laboratory tests using the flight hardware. These calibration data should be employed in the ground processing of the actual sensor measurements to achieve the best possible attitude pointing knowledge. The residual angular biases in the sensor measurement

Received 20 May 2005; revision received 17 September 2005; accepted for publication 20 September 2005.

*Consultant; jvdha@aol.com. Senior Member AIAA.

angles are typically only a few hundredths of a degree and are negligible in practice.

After the sensor calibration data are incorporated, the following principal sources of biases remain: 1) spacecraft dynamic imbalance effects, 2) misalignments of the sensor box relative to the spacecraft, and 3) systematic errors in the effective Earth's infrared radius.

Seasonal influences (in particular, the north–south thermal gradient) produce asymmetrical biases in the Earth's radiation profile that lead to systematic errors in the crossings of the Earth's infrared disk measured by the Earth sensor detectors. Other biases, for instance, in sun ephemeris and orbit-determination knowledge, are usually of the order of a few hundredths of a degree and may be neglected in comparison to the errors considered here.

A model is presented for the propagation of the dominant systematic biases through the attitude-determination algorithm. The model is useful for establishing, during the spacecraft design phase, a realistic budget for the attitude-determination error on the basis of the predicted statistical properties of the input biases. Finally, the model identifies the basic relationships between the individual biases and the individual sensor measurement angles. These insights lead naturally to a system of equations that can be used in an operational procedure for determining the individual biases from the observed measurement residuals. The application of the model is illustrated using the actual parameters and measurements of the CONTOUR spacecraft during its phasing orbits in August 2002.

II. Geometrical Bias Model

A. Assumptions

The effects induced by the biases will be formulated in terms of a linear, that is, first-order, model that will be established over an interval of time corresponding to a single spacecraft spin revolution. Considering the specific objective as well as the time frame of this approximate model, we may adopt the following operational conditions:

1) Disturbance and control torques are assumed to be absent, and so the angular momentum vector can be considered fixed in inertial space

2) The spacecraft is performing a pure spin about its dynamic spin axis, that is, the maximum or minimum axis of inertia, so that nutational effects are assumed to be absent

3) The spacecraft spin rate is assumed constant (typically, in the interval between 10 and 60 rpm)

4) The sun's position as seen from the spacecraft is taken fixed in inertial space

5) Also the Earth's position as seen from the spacecraft is taken fixed in inertial space in the present analysis; although the Earth's motion may be appreciable during a single spacecraft spin revolution, that is, up to 0.4 deg for a spacecraft in low Earth orbit at a 10-rpm spin rate, the assumption is justified for the purpose of evaluating the effects of the small biases on the resulting attitude solution in a first-order analysis.

B. Sun and Earth Vectors in Principal Frame

In the absence of nutation, a spinning spacecraft will naturally perform a pure spin rotational motion around its maximum or minimum principal inertia axis. Figure 1 shows the relevant geometry with the actual (positive) spin axis along the principal inertia axis Z_p. The plane formed by this axis and the sun vector is fixed in inertial space under the adopted conditions. Therefore, it is meaningful to introduce the inertial reference axes X_i, Y_i, and Z_i.

1) The Z_i axis coincides with the Z_p axis, that is, the actual (dynamic) spacecraft spin axis.

2) The X_i axis is taken within the plane containing the sun vector and the Z_p axis; it remains fixed in inertial space but lies always within the spacecraft equator, that is, the plane that is normal to the spin axis and contains the spacecraft center of mass.

3) The Y_i axis completes the coordinate triad, lies also within the spacecraft equator, and is fixed in inertial space.

The sun unit vector $\boldsymbol{S}$ points from the spacecraft to the sun and forms a constant angle, (that is, the sun aspect angle β_S in Fig. 1)

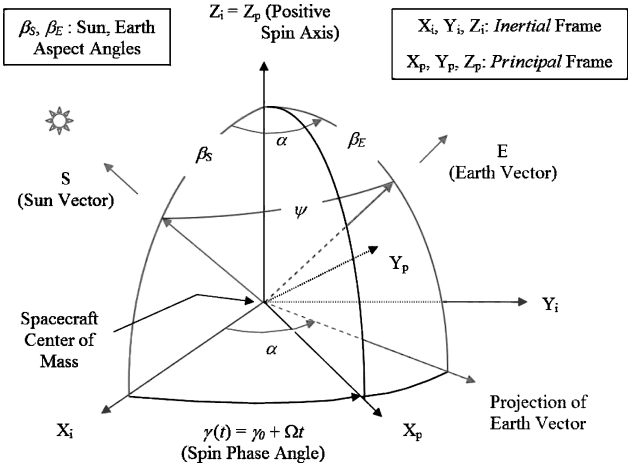

Fig. 1 Geometry of sun, Earth, and spacecraft principal frame.

with the unit vector $\boldsymbol{Z}_p$ along the dynamic spin axis,

$$\beta_S = \arccos\{\boldsymbol{S} \cdot \boldsymbol{Z}_p\} \tag{1}$$

The projection of the sun vector in the spacecraft's equatorial plane coincides with the X_i axis, and its components in the inertial reference frame (X_i, Y_i, Z_i) are

$$\boldsymbol{S}_i = (\sin\beta_S, 0, \cos\beta_S)^T \tag{2}$$

The unit vector $\boldsymbol{E}$ points in the direction of the instantaneous Earth center and forms a constant angle with the spacecraft dynamic spin axis (under the preceding assumptions), that is, the Earth aspect angle β_E shown in Fig. 1,

$$\boldsymbol{E} \cdot \boldsymbol{Z}_p = \cos\beta_E \tag{3}$$

The components of the Earth vector in the adopted inertial reference frame (X_i, Y_i, Z_i) are

$$\boldsymbol{E}_i = (\sin\beta_E \cos\alpha, \sin\beta_E \sin\alpha, \cos\beta_E)^T \tag{4}$$

The angle α is the sun–Earth dihedral angle, which represents the rotation angle (about the dynamic spin axis) from the sun spin axis plane to the Earth spin axis plane (Fig. 1). The sun–Earth angle $\psi = \arccos(\boldsymbol{S} \cdot \boldsymbol{E})$ is shown in Fig. 1 and is independent of the attitude orientation. The angles β_S, β_E, α, and ψ are interrelated (from spherical geometry) by

$$\cos\psi = \cos\beta_S \cos\beta_E + \sin\beta_S \sin\beta_E \cos\alpha \tag{5}$$

This result may be used as a check on the consistency of the measurement angles β_S, β_E, and α.

The plane formed by the spacecraft principal X_p and Z_p axes in Fig. 1 performs a uniform rotation about the Z_p axis with spin rate Ω and instantaneous spin phase angle $\gamma(t) = \gamma_0 + \Omega t$ relative to the inertial (X_i, Z_i) frame with initial phase angle γ_0. The spin rate Ω about the Z_p axis is positive and constant within the context of the adopted assumptions.

On the basis of the geometry in Fig. 1 and the preceding results we can express the sun vector $\boldsymbol{S}_i$ of Eq. (2) in terms of its components in the spacecraft principal (X_p, Y_p, Z_p) frame,

$$\boldsymbol{S}_p = \begin{pmatrix} S_{p1} \\ S_{p2} \\ S_{p3} \end{pmatrix} = [R(\gamma)]\,\boldsymbol{S}_i = \begin{pmatrix} \sin\beta_S \cos\gamma(t) \\ -\sin\beta_S \sin\gamma(t) \\ \cos\beta_S \end{pmatrix} \tag{6}$$

where $[R(\gamma)]$ is the rotation matrix from the inertial to the spacecraft principal frame,

$$[R(\gamma)] = \begin{bmatrix} \cos\gamma(t) & \sin\gamma(t) & 0 \\ -\sin\gamma(t) & \cos\gamma(t) & 0 \\ 0 & 0 & 1 \end{bmatrix} \tag{7}$$

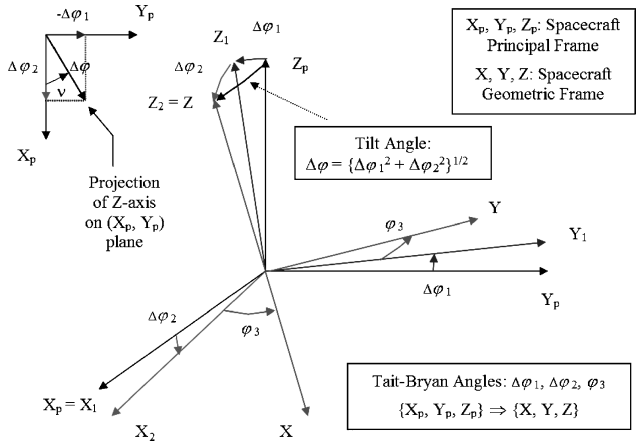

Fig. 2 Transformation from principal to geometric reference frames.

In a similar manner, the inertial representation of the Earth vector $\boldsymbol{E}_i$ in Eq. (4) can be transformed to its components in the spacecraft principal frame,

$$\boldsymbol{E}_p = \begin{bmatrix} E_{p1} \\ E_{p2} \\ E_{p3} \end{bmatrix} = [R(\gamma)]\,\boldsymbol{E}_i = \begin{pmatrix} \sin\beta_E \cos\{\gamma(t) - \alpha\} \\ -\sin\beta_E \sin\{\gamma(t) - \alpha\} \\ \cos\beta_E \end{pmatrix} \tag{8}$$

At the instant t_E when $\gamma(t_E)$ equals α, we find $\boldsymbol{E}_p = (\sin\beta_E, 0, \cos\beta_E)^T$ as can be seen in Fig. 1.

C. Dynamic Imbalance

The dynamic imbalance [also known as coning (Wertz,[4] p. 489)] is one of the most significant bias errors affecting the attitude-determination accuracy. The imbalance refers to the angular deviation between the following two reference directions (Fig. 2): 1) the actual or dynamic spin axis, which corresponds to the maximum or minimum principal axis of inertia, and 2) the geometric spin axis or centerline, which represents the intended spin axis orientation (during the design phase).

The mounting and alignment of the sensor units during pre launch spacecraft integration are performed with reference to the spacecraft geometric reference frame. During in-flight operations, however, the spacecraft actually spins about the dynamic spin axis Z_p. The offset with the geometric spin axis alters the effective inertial pointing direction of the sensors and contaminates the sensor measurements.

The transformation between the spacecraft geometric frame (X, Y, Z) and the principal reference frame (X_p, Y_p, Z_p) will now be described by the small Tait–Bryan rotation angles $\Delta\varphi_1$ and $\Delta\varphi_2$ followed by the phase angle φ_3 (Fig. 2). The angles $\Delta\varphi_1$ and $\Delta\varphi_2$ represent the components of the projection of the geometric spin axis Z within the plane normal to the dynamic spin axis Z_p. These angles are not known in actual practice; otherwise, an effort would be done to eliminate them. Therefore, the biases $\Delta\varphi_1$ and $\Delta\varphi_2$ may be reasonably modeled as normally distributed random variables with expected values equal to zero. Their variances may be predicted from the expected precision of the prelaunch balancing tests while also accounting for any in-flight error sources (in particular, the imbalance induced by an asymmetric use of propellant in the tanks).

The third rotation over φ_3 is about the spacecraft geometric Z axis and represents the phase angle of the geometric X axis with respect to the principal X_p axis. Also this angle may have a bias error caused by limitations in the balancing precision. For spacecraft with almost symmetric planar moments of inertia $I_x \approx I_y$, the locations of the planar principal axes are very sensitive to small variations in the assumed mass model so that the phase angle φ_3 can be relatively large. Thus, the assumption that the angle φ_3 is small may not be justified in this case, and the angle φ_3 may be reasonably modeled as a random variable that may take any value within the interval (0, 360) deg.

The small rotations $\Delta\varphi_1$ and $\Delta\varphi_2$ are expressed by the rotation matrices $[R_1]$ and $[R_2]$ and the rotation over the phase angle φ_3 is denoted by $[R_3]$,

$$[R_1(\Delta\varphi_1)] = \begin{bmatrix} 1 & 0 & 0 \\ 0 & \cos\Delta\varphi_1 & \sin\Delta\varphi_1 \\ 0 & -\sin\Delta\varphi_1 & \cos\Delta\varphi_1 \end{bmatrix}$$

$$\approx \begin{bmatrix} 1 & 0 & 0 \\ 0 & 1 & \Delta\varphi_1 \\ 0 & -\Delta\varphi_1 & 1 \end{bmatrix} \tag{9a}$$

$$[R_2(\Delta\varphi_2)] = \begin{bmatrix} \cos\Delta\varphi_2 & 0 & -\sin\Delta\varphi_2 \\ 0 & 1 & 0 \\ \sin\Delta\varphi_2 & 0 & \cos\Delta\varphi_2 \end{bmatrix}$$

$$\approx \begin{bmatrix} 1 & 0 & -\Delta\varphi_2 \\ 0 & 1 & 0 \\ \Delta\varphi_2 & 0 & 1 \end{bmatrix} \tag{9b}$$

$$[R_3(\varphi_3)] = \begin{bmatrix} \cos\varphi_3 & \sin\varphi_3 & 0 \\ -\sin\varphi_3 & \cos\varphi_3 & 0 \\ 0 & 0 & 1 \end{bmatrix} \tag{9c}$$

It is convenient to employ a polar notation with $\Delta\varphi$ denoting the tilt angle between the geometric Z axis and the principal Z_p axis and ν representing an unknown fixed phase angle of the tilt angle offset with respect to the X_p axis (inset Fig. 2). Because $\Delta\varphi_1$ equals $-\Delta\varphi \sin\nu$ and $\Delta\varphi_2 = \Delta\varphi\cos\nu$, we have

$$\Delta\varphi = \left\{(\Delta\varphi_1)^2 + (\Delta\varphi_2)^2\right\}^{\frac{1}{2}}, \qquad \nu = \arctan\{-\Delta\varphi_1/\Delta\varphi_2\} \tag{10}$$

The statistical properties of the tilt angle $\Delta\varphi$ follow naturally from those of the individual imbalance components: $\sigma_\varphi^2 = E\{(\Delta\varphi)^2\} = 2\sigma^2$ with $\sigma^2 = E\{(\Delta\varphi_1)^2\} = E\{\Delta\varphi_2)\}^2$. The tilt phase angle ν is assumed to be uniformly distributed over the interval (0, 360) deg. The small-angle approximations used in Eqs. (9a) and (9b) are justified on the grounds that the tilt angle is very small (typically, $\Delta\varphi < 0.1$ deg).

The transformation from the principal to the geometric frame is given by

$$\begin{pmatrix} X \\ Y \\ Z \end{pmatrix} = [R_3(\varphi_3)][R_2(\Delta\varphi_2)][R_1(\Delta\varphi_1)] \begin{pmatrix} X_p \\ Y_p \\ Z_p \end{pmatrix}$$

$$= [R_{\text{tilt}}(\varphi_3, \nu, \Delta\varphi)] \begin{pmatrix} X_p \\ Y_p \\ Z_p \end{pmatrix} \tag{11}$$

The small-angle representation of the tilt matrix $[R_{\text{tilt}}]$ follows from Eqs. (9–11),

$$[R_{\text{tilt}}(\varphi_3, \nu, \Delta\varphi)] \approx \begin{bmatrix} \cos\varphi_3 & \sin\varphi_3 & -\Delta\varphi\cos(\nu - \varphi_3) \\ -\sin\varphi_3 & \cos\varphi_3 & -\Delta\varphi\sin(\nu - \varphi_3) \\ \Delta\varphi\cos\nu & \Delta\varphi\sin\nu & 1 \end{bmatrix} \tag{12}$$

Both ν and $\nu - \varphi_3$ have uniform probability distributions over the interval (0, 360) deg. The arbitrariness in these angles has no implications on the attitude-determination process because the instant when the sun crosses the sensor meridian plane will be taken as the reference for all sensor measurements [to be discussed following Eq. (23)].

Finally, it can be shown that the rotation matrices defined in Eqs. (9) are orthonormal (up to first-order terms) and may be inverted by transposing them. The same holds true for the matrix in Eq. (12) because of the adopted small-angle model.

D. Sensor Frame Within Geometrical Frame

The actual measurements produced by the Earth sun sensor are carefully calibrated by dedicated laboratory tests. This ensures that the measurement angles will be accurate to within a few hundredths of a degree over the specified operating range of the sensor. The calibration results effectively eliminate any sensor-internal mechanical misalignments, as well as any systematic errors originating in the electronics and processing units. The sensor calibration data are referred to the sensor-fixed reference frame that is attached to the reflecting cube mounted on top of the sensor box (Fig. 3). This cube serves as the reference for the precise alignment of the sensor box within the spacecraft reference frame during spacecraft integration.

Because of inherent limitations in the alignment precision and other error effects, there may be a mounting misalignment (typically, <0.1 deg) between the sensor box and the spacecraft geometric reference frame. The pointing axis $X_{\rm sb}$ of the sensor box lies in the spacecraft geometric (X, Y) plane with nominal phase angle $\chi_{\rm sb}$ with respect to the spacecraft X axis (Fig. 4). The sensor alignment biases that will be employed here are the three small angles $\Delta\chi$, Δe, and Δi,

1) The bias $\Delta\chi$ designates the error in the equatorial mounting angle χ. It consists of a rotation about the spacecraft geometric Z axis resulting in the intermediate X_1 and Y_1 axes. The $\Delta\chi$ angle can be interpreted as an azimuth error in the sensor-pointing direction within the (X, Y) plane, which leads to constant offsets in all sun and Earth sensor crossing times.

2) The bias Δe models the error in the sensor-mounting alignment in the direction normal to the spacecraft equatorial plane and is described by a rotation about the negative Y_1 axis resulting in the new X_2 and Z_2 axes. This bias can be interpreted as an elevation error in the sensor-pointing direction, which leads to an offset in the intersection of the sun sensor meridian and skew slits and to biases in the effective pencil-beam mounting angles, thereby affecting the sun and Earth aspect angle measurements.

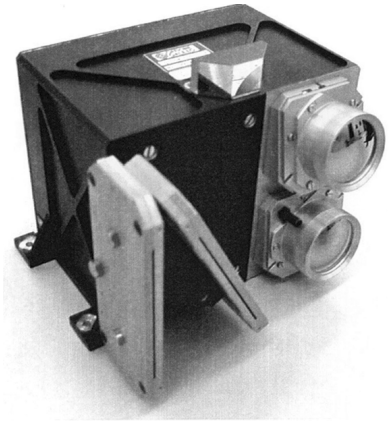

Fig. 3 Integrated Earth sun sensor.

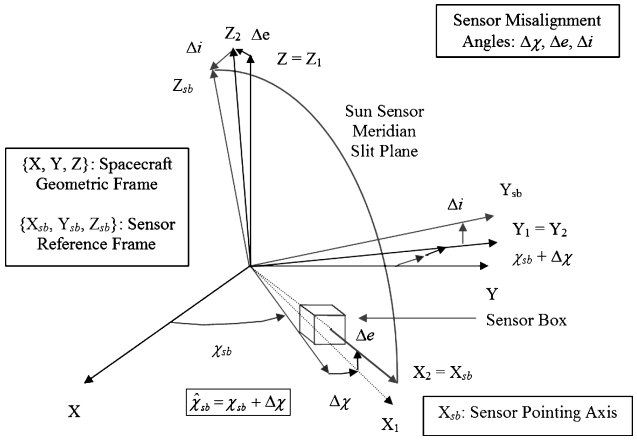

Fig. 4 Sensor-mounting misalignment in spacecraft geometric frame.

3) The bias Δi represents an inclination error in the sensor orientation induced by a rotation about the sensor-pointing direction, that is, axis $X_2 = X_{\rm sb}$. This bias leads to a change in the inclination of the sun sensor slit plane, which affects the resulting sun aspect angle in an intricate manner. It also affects the pencil-beam orientations and the measurements of the sun–Earth dihedral angle.

The complete transformation (in first-order small angle approximation) from the spacecraft geometric reference frame (X, Y, Z) to the sensor reference frame $(X_{\rm sb}, Y_{\rm sb}, Z_{\rm sb})$ may be formulated as

$$\begin{pmatrix} X_{\rm sb} \\ Y_{\rm sb} \\ Z_{\rm sb} \end{pmatrix} = [R_{\rm sb}(\chi_{\rm sb}, \Delta\chi, \Delta e, \Delta i)] \begin{pmatrix} X \\ Y \\ Z \end{pmatrix} \tag{13}$$

The sensor misalignment matrix $[R_{\rm sb}]$ is defined by

$$[R_{\rm sb}] = [R_i(\Delta i)][R_e(\Delta e)][R_\chi(\chi_{\rm sb}, \Delta\chi)] \tag{14}$$

with

$$[R_\chi(\chi_{\rm sb}, \Delta\chi)] = \begin{bmatrix} \cos(\chi_{\rm sb}+\Delta\chi) & \sin(\chi_{\rm sb}+\Delta\chi) & 0 \\ -\sin(\chi_{\rm sb}+\Delta\chi) & \cos(\chi_{\rm sb}+\Delta\chi) & 0 \\ 0 & 0 & 1 \end{bmatrix} \tag{15a}$$

$$[R_e(\Delta e)] = \begin{bmatrix} \cos\Delta e & 0 & \sin\Delta e \\ 0 & 1 & 0 \\ -\sin\Delta e & 0 & \cos\Delta e \end{bmatrix} \approx \begin{bmatrix} 1 & 0 & \Delta e \\ 0 & 1 & 0 \\ -\Delta e & 0 & 1 \end{bmatrix} \tag{15b}$$

$$[R_i(\Delta i)] = \begin{bmatrix} 1 & 0 & 0 \\ 0 & \cos\Delta i & \sin\Delta i \\ 0 & -\sin\Delta i & \cos\Delta i \end{bmatrix} \approx \begin{bmatrix} 1 & 0 & 0 \\ 0 & 1 & \Delta i \\ 0 & -\Delta i & 1 \end{bmatrix} \tag{15c}$$

An expansion of the matrix in Eq. (15a) for small angles $\Delta\chi$ is not necessary because the bias $\Delta\chi$ appears only in combination with the $\chi_{\rm sb}$ angle. Therefore, we employ the new angular variable $\hat{\chi}_{\rm sb} = \chi_{\rm sb} + \Delta\chi$. The sensor misalignment matrix $[R_{\rm sb}]$ takes now the form

$$[R_{\rm sb}(\hat{\chi}_{\rm sb}, \Delta e, \Delta i)] \approx \begin{bmatrix} \cos\hat{\chi}_{\rm sb} & \sin\hat{\chi}_{\rm sb} & \Delta e \\ -\sin\hat{\chi}_{\rm sb} & \cos\hat{\chi}_{\rm sb} & \Delta i \\ \Delta i\sin\hat{\chi}_{\rm sb} - \Delta e\cos\hat{\chi}_{\rm sb} & -\Delta i\cos\hat{\chi}_{\rm sb} - \Delta e\sin\hat{\chi}_{\rm sb} & 1 \end{bmatrix} \tag{16}$$

Also this matrix is orthonormal within the small-angle approximations adopted here.

E. Sun Vector in Sensor Frame

To establish the measurement equations for the sun sensor we must transform the sun vector $\boldsymbol{S}_p = (S_{p1}, S_{p2}, S_{p3})^T$ from Eq. (6) to the sensor reference frame $(X_{\rm sb}, Y_{\rm sb}, Z_{\rm sb})$. The sun vector components within the latter frame are written as $\boldsymbol{S}_{\rm sb} = (S_{\rm sb1}, S_{\rm sb2}, S_{\rm sb3})^T$. The transformation follows from the results established in Eqs. (11–16) and uses the sun vector components $\boldsymbol{S}_{\rm geom} = (S_X, S_Y, S_Z)^T$ within the intermediate spacecraft geometric frame,

$$\boldsymbol{S}_{\rm sb} = \begin{pmatrix} S_{\rm sb1} \\ S_{\rm sb2} \\ S_{\rm sb3} \end{pmatrix} = [R_{\rm sb}] \begin{pmatrix} S_X \\ S_Y \\ S_Z \end{pmatrix} = [R_{\rm sb}][R_{\rm tilt}] \begin{pmatrix} S_{p1} \\ S_{p2} \\ S_{p3} \end{pmatrix} \tag{17}$$

F. Ideal Sun Vector

The sun vector $\boldsymbol{S}_{\rm sb}$ may be split up in an ideal part, which holds when the sensor biases Δe and Δi are absent, and a perturbing part induced by the biases Δe and Δi,

$$\boldsymbol{S}_{\rm sb} = \boldsymbol{S}_{\rm sb,\,ideal} + \boldsymbol{S}_{\rm sb,\,pert} \tag{18}$$

The ideal and perturbation parts of the matrix $[R_{\rm sb}(\hat{\chi}_{\rm sb}, \Delta e, \Delta i)]$ follow from Eq. (16),

$$[R_{\rm sb,\ ideal}(\hat{\chi}_{\rm sb})] = \begin{bmatrix} \cos\hat{\chi}_{\rm sb} & \sin\hat{\chi}_{\rm sb} & 0 \\ -\sin\hat{\chi}_{\rm sb} & \cos\hat{\chi}_{\rm sb} & 0 \\ 0 & 0 & 1 \end{bmatrix} \tag{19a}$$

$$[R_{\rm sb,\ pert}(\hat{\chi}_{\rm sb}, \Delta e, \Delta i)] = \begin{bmatrix} 0 & 0 & \Delta e \\ 0 & 0 & \Delta i \\ \Delta i \sin\hat{\chi}_{\rm sb} - \Delta e\cos\hat{\chi}_{\rm sb} & -\Delta i\cos\hat{\chi}_{\rm sb} - \Delta e\sin\hat{\chi}_{\rm sb} & 0 \end{bmatrix} \tag{19b}$$

Also the tilt matrix $[R_{\rm tilt}(\varphi_3, \nu, \Delta\varphi)]$ of Eq. (12) may be expanded similarly,

$$[R_{\rm tilt,\ ideal}(\varphi_3)] = \begin{bmatrix} \cos\varphi_3 & \sin\varphi_3 & 0 \\ -\sin\varphi_3 & \cos\varphi_3 & 0 \\ 0 & 0 & 1 \end{bmatrix} \tag{20a}$$

$$[R_{\rm tilt,\ pert}(\varphi_3, \nu, \Delta\varphi)] = \begin{bmatrix} 0 & 0 & -\Delta\varphi\cos(\nu-\varphi_3) \\ 0 & 0 & -\Delta\varphi\sin(\nu-\varphi_3) \\ \Delta\varphi\cos\nu & \Delta\varphi\sin\nu & 0 \end{bmatrix} \tag{20b}$$

The matrix $[R_{\rm ideal}(\varphi_3, \hat{\chi}_{\rm sb})]$ equals the product of the matrices $[R_{\rm sb,\ ideal}(\hat{\chi}_{\rm sb})]$ and $[R_{\rm tilt,\ ideal}(\varphi_3)]$ in Eqs. (19a) and (20a),

$$[R_{\rm ideal}(\varphi_3, \hat{\chi}_{\rm sb})] = \begin{bmatrix} \cos(\varphi_3+\hat{\chi}_{\rm sb}) & \sin(\varphi_3+\hat{\chi}_{\rm sb}) & 0 \\ -\sin(\varphi_3+\hat{\chi}_{\rm sb}) & \cos(\varphi_3+\hat{\chi}_{\rm sb}) & 0 \\ 0 & 0 & 1 \end{bmatrix} \tag{21}$$

The ideal sun vector in sensor frame coordinates follows now from Eqs. (17) and (6),

$$\boldsymbol{S}_{\rm sb,\ ideal} = \begin{pmatrix} S_{\rm sb1} \\ S_{\rm sb2} \\ S_{\rm sb3} \end{pmatrix}_{\rm ideal} = [R_{\rm ideal}(\varphi_3, \hat{\chi}_{\rm sb})] \begin{pmatrix} S_{p1} \\ S_{p2} \\ S_{p3} \end{pmatrix} = \begin{pmatrix} \sin\beta_S\cos\tilde{\gamma}(t) \\ -\sin\beta_S\sin\tilde{\gamma}(t) \\ \cos\beta_S \end{pmatrix} \tag{22}$$

with

$$\tilde{\gamma}(t) = \gamma(t) + \varphi_3 + \hat{\chi}_{\rm sb} = \tilde{\gamma}_0 + \Omega t \tag{23}$$

The angle $\tilde{\gamma}(t)$ describes the time-varying phase of the $(X_{\rm sb}, Z_{\rm sb})$ plane relative to the inertial X_i axis (Figs. 1–4) and $\tilde{\gamma}_0 = \gamma_0 + \varphi_3 + \hat{\chi}_{\rm sb}$. It is convenient to select the time origin as the instant at which the sun vector crosses the $(X_{\rm sb}, Z_{\rm sb})$ plane, which coincides with the sun sensor's meridian slit plane,

$$\tilde{\gamma}(t) = \Omega t \rightarrow \tilde{\gamma}_0 = \tilde{\gamma}(t=0) = 0, \qquad \gamma_0 = -(\varphi_3 + \hat{\chi}_{\rm sb}) \tag{24}$$

G. Sun Vector in Presence of Biases

The perturbation term of the sun vector coordinates in the sensor frame comes from Eq. (17),

$$\boldsymbol{S}_{\rm sb,\ pert} = [R_{\rm pert}(\hat{\chi}_{\rm sb}, \Delta e, \Delta i, \varphi_3, \nu, \Delta\varphi)]\boldsymbol{S}_p \tag{25}$$

with

$$[R_{\rm pert}] \approx [R_{\rm sb,\ ideal}(\hat{\chi}_{\rm sb})][R_{\rm tilt,\ pert}(\varphi_3, \nu, \Delta\varphi)] + [R_{\rm sb,\ pert}(\hat{\chi}_{\rm sb}, \Delta e, \Delta i)][R_{\rm tilt,\ ideal}(\varphi_3)] \tag{26}$$

The vector $\boldsymbol{S}_{\rm sb,\ pert}$ can be calculated in explicit form from the results in Eqs. (19) and (20),

$$\boldsymbol{S}_{\rm sb,\ pert} \approx \begin{pmatrix} -\cos\beta_S(\Delta\varphi\cos\tilde{\chi} - \Delta e) \\ \cos\beta_S(\Delta\varphi\sin\tilde{\chi} + \Delta i) \\ \sin\beta_S\{(\Delta\varphi\cos\tilde{\chi} - \Delta e)\cos\tilde{\gamma}(t) + (\Delta\varphi\sin\tilde{\chi} + \Delta i)\sin\tilde{\gamma}(t)\} \end{pmatrix} \tag{27}$$

The angle $\tilde{\chi}$ appearing here stands for

$$\tilde{\chi} = \varphi_3 + \hat{\chi}_{\rm sb} - \nu \tag{28}$$

Geometrically, $\tilde{\chi}$ represents the constant (but unknown) phase angle between the sensor pointing direction $X_{\rm sb}$ and the projection of the geometric Z axis on the principal (X_p, Y_p) plane (Figs. 1–4).

The result in Eq. (27) can be simplified by introducing a combination of the sensor alignment biases with the tilt angle components. This is achieved by rotating the phase of the projected Z axis (Fig. 2) to the sensor-pointing direction $X_{\rm sb}$ using the angle $\tilde{\chi}$,

$$\Delta\varphi_e = \Delta\varphi\cos\tilde{\chi} + \Delta e, \qquad \Delta\varphi_i = \Delta\varphi\sin\tilde{\chi} + \Delta i \tag{29}$$

Finally, the result for $\boldsymbol{S}_{\rm sb} = \boldsymbol{S}_{\rm sb,\ ideal} + \boldsymbol{S}_{\rm sb,\ pert}$ can be rewritten in terms of the generalized tilt matrix $[T]$ and the ideal sun vector in Eq. (22),

$$\boldsymbol{S}_{\rm sb} \approx [I + T(\Delta\varphi_e, \Delta\varphi_i)]\boldsymbol{S}_{\rm sb,\ ideal} \tag{30}$$

where I is the identity matrix and $[T]$ is defined by

$$[T(\Delta\varphi_e, \Delta\varphi_i)] = \begin{bmatrix} 0 & 0 & -\Delta\varphi_e \\ 0 & 0 & \Delta\varphi_i \\ \Delta\varphi_e & -\Delta\varphi_i & 0 \end{bmatrix} \tag{31}$$

H. Earth Vector in Presence of Biases

The expression for the instantaneous Earth vector $\boldsymbol{E}$ in terms of its components in the sensor frame may be established similarly as was done for the sun vector [Eq. (17)] by using the Earth vector components $\boldsymbol{E}_p$ in Eq. (8),

$$\boldsymbol{E}_{\rm sb} = \begin{pmatrix} E_{\rm sb1} \\ E_{\rm sb2} \\ E_{\rm sb3} \end{pmatrix} \approx [R_{\rm sb}(\hat{\chi}_{\rm sb}, \Delta e, \Delta i)] \begin{pmatrix} E_X \\ E_Y \\ E_Z \end{pmatrix} \approx [R_{\rm sb}(\hat{\chi}_{\rm sb}, \Delta e, \Delta i)][R_{\rm tilt}(\varphi_3, \nu, \Delta\varphi)] \begin{pmatrix} E_{p1} \\ E_{p2} \\ E_{p3} \end{pmatrix} \tag{32}$$

After expanding the matrix-product in an ideal term and a perturbation part, we find as in Eqs. (22–27),

$$\boldsymbol{E}_{\rm sb,\ ideal} = [R_{\rm ideal}]\boldsymbol{E}_p = \begin{pmatrix} \sin\beta_E\cos\{\tilde{\gamma}(t) - \alpha\} \\ -\sin\beta_E\sin\{\tilde{\gamma}(t) - \alpha\} \\ \cos\beta_E \end{pmatrix} \boldsymbol{E}_p \tag{33a}$$

$$\boldsymbol{E}_{\rm sb,\ pert} = [R_{\rm pert}]\boldsymbol{E}_p \approx \begin{pmatrix} -\Delta\varphi_e\cos\beta_E \\ \Delta\varphi_i\cos\beta_E \\ \sin\beta_E\{\Delta\varphi_e\cos[\tilde{\gamma}(t) - \alpha] + \Delta\varphi_i\sin[\tilde{\gamma}(t) - \alpha]\} \end{pmatrix} \boldsymbol{E}_p \tag{33b}$$

The final result for $\boldsymbol{E}_{\rm sb} = \boldsymbol{E}_{\rm sb,\ ideal} + \boldsymbol{E}_{\rm sb,\ pert}$ can be expressed in a similar way as was done for $\boldsymbol{S}_{\rm sb}$ in Eq. (30),

$$\boldsymbol{E}_{\rm sb} \approx [I + T(\Delta\varphi_e, \Delta\varphi_i)]\boldsymbol{E}_{\rm sb,\ ideal} \tag{34}$$

Table 1 Summary of sun and Earth sensor measurements

	Sun sensor		Earth sensor	
Sensor outputs	Measurement 1	Measurement 2	Measurement 3	Measurement 4
Crossing designation	Meridian Slit	Skew Slit	In (space–Earth)	Out (Earth–space)
Crossing time	t_1	t_2	t_3	t_4
Spin phase angle $\tilde{\gamma}_j(t)$	$\tilde{\gamma}_1 = \tilde{\gamma}_0 + \Omega t_1$	$\tilde{\gamma}_2 = \tilde{\gamma}_0 + \Omega t_2$	$\tilde{\gamma}_{\text{in}} = \tilde{\gamma}_0 + \Omega t_3$	$\tilde{\gamma}_{\text{out}} = \tilde{\gamma}_0 + \Omega t_4$
Angular observations	Reference	$\tilde{\gamma}_2 - \tilde{\gamma}_1$	$\tilde{\gamma}_{\text{in}} - \tilde{\gamma}_1$	$\tilde{\gamma}_{\text{out}} - \tilde{\gamma}_1$
Matching attitude state	Spin rate	Sun angle	Angle $\alpha - \kappa$	Angle $\alpha + \kappa$

III. Sensor Measurement Model

A. Background and Approach

During each spacecraft spin revolution the following Sun and Earth sensor measurements are generated[3]: 1) the time t_1 when the sun crosses the sun sensor's meridian slit, 2) the time t_2 when the sun crosses the sensor's skew slit, 3) the Earth sensor "in" crossing time t_3 (when the pencil beam crosses the Earth's infrared horizon in the space to Earth direction), and 4) the Earth sensor "out" crossing time t_4 (when the pencil beam crosses the Earth's infrared horizon from Earth to space).

The meridian slit crossing time t_1 is used as the reference for the other sensor measurements. Successive meridian slit crossing times allow the calculation of the spin rate, which is needed for the conversion of the observed crossing times into angular observations. Table 1 summarizes the sensor measurements and their associated attitude parameters.

The angles $\tilde{\gamma}_{\text{in}} = \tilde{\gamma}(t_3)$ and $\tilde{\gamma}_{\text{out}} = \tilde{\gamma}(t_4)$ represent the phase angles of the pencil-beam in and out crossings relative to the inertial (X_i, Z_i) plane. The pencil-beam measurements that are actually used in the attitude determination process are the rotation angles $\tilde{\gamma}_{\text{in}} - \tilde{\gamma}_1$ and $\tilde{\gamma}_{\text{out}} - \tilde{\gamma}_1$, which are referred to the occurrence of the meridian slit pulse. This observation is immaterial in the ideal case but is important when biases are acting because they introduce an offset $\Delta\tilde{\gamma}_1$ in the actual occurrence of the sun meridian pulse.

The following approach will be adopted.

1) In the first step, the ideal situation, that is, in the absence of the generalized biases $\Delta\varphi_e$ and $\Delta\varphi_i$, is considered and the crossing conditions are formulated in terms of $\boldsymbol{S}_{\text{sb,ideal}}$ and $\boldsymbol{E}_{\text{sb,ideal}}$. This produces the ideal results for the crossing angles $\tilde{\gamma}_{j,\text{ideal}}$, for $j = 1, \ldots, 4$.

2) Subsequently, the perturbed situation, that is, in the presence of the biases $\Delta\varphi_e$ and $\Delta\varphi_i$, is studied with inclusion of the terms $\boldsymbol{S}_{\text{sb,pert}}$ and $\boldsymbol{E}_{\text{sb,pert}}$ in the crossing conditions to model the changes in these vectors induced by the biases. The crossing angle solutions are then expressed as $\tilde{\gamma}_j = \tilde{\gamma}_{j,\text{ideal}} + \Delta\tilde{\gamma}_j$ with the small correction term $\Delta\tilde{\gamma}_j$ accounting for the bias effects. Finally, the resulting crossing equations are solved by means of a first-order perturbation analysis for $\Delta\tilde{\gamma}_j$ representing the offsets in the angular measurements induced by the biases.

B. Sun Sensor Measurements

Meridian Slit Crossings

Sun crossings over the meridian slit of the sun sensor occur at the instants when the sun vector coincides with the plane of the meridian slit, that is, the (X_{sb}, Z_{sb}) plane in Fig. 4. This occurrence is expressed by the necessary condition that the normal $\boldsymbol{n}_1 = \boldsymbol{Y}_{\text{sb}}$ to the meridian slit plane (where 1 identifies the sun sensor's meridian slit) must be perpendicular to the sun vector at the crossing instant,

$$(\boldsymbol{n}_1 \cdot \boldsymbol{S}_{\text{sb}}) = (\boldsymbol{Y}_s \cdot \boldsymbol{S}_{\text{sb}}) = 0 \tag{35}$$

In practice, there are additional constraints that must be satisfied for the sun sensor to produce valid outputs. (Typically, the sun aspect angle must be between about 60 and 150 deg.)

In the ideal case, the condition expressed by Eq. (35) together with $\boldsymbol{S}_{\text{sb, ideal}}$ in Eq. (22) lead to the known trivial solution for the meridian slit crossing angle,

$$\sin\beta_S \sin\tilde{\gamma}(t_{1,\text{ideal}}) = 0 \rightarrow \tilde{\gamma}_{1,\text{ideal}} = \tilde{\gamma}(t_{1,\text{ideal}}) = 0, \qquad t_{1,\text{ideal}} = 0 \tag{36}$$

In practice, nonzero biases may be acting, and the more general sun vector expressions in Eqs. (25–30) should be used. The meridian slit crossing angle $\tilde{\gamma}_1$ may be expanded in terms of the ideal solution $\tilde{\gamma}_{1,\text{ideal}}$ plus a small correction term $\Delta\tilde{\gamma}_1$ caused by the biases. After substituting this expansion into the crossing condition (35), we find the small-angle result,

$$\sin\beta_S \sin(\tilde{\gamma}_{1,\text{ideal}} + \Delta\tilde{\gamma}_1) - \Delta\varphi_i \cos\beta_S = 0 \rightarrow \Delta\tilde{\gamma}_1 \cong \Delta\varphi_i / \tan\beta_S \tag{37}$$

This result represents the shift $\Delta\tilde{\gamma}_1$ in the meridian slit crossing angle caused by the biases, and this shift must be taken into account when analyzing the other measurements (Table 1).

It is evident from Eqs. (29) that the expected value of the correction term vanishes based on the fact that both biases Δi and $\Delta\varphi$ have expected values of zero. Because the phase angle φ_3–ν is uniformly distributed over the interval (0, 360 deg) the angle $\tilde{\chi}$ defined in Eq. (28) also has a uniform distribution so the expected value of $(\sin\tilde{\chi})^2 = 0.5$. The variance of the crossing angle $\Delta\tilde{\gamma}_1$ in result (37) can, thus, be expressed in terms of the variances of the individual biases,

$$\sigma_1^2 = E\left\{(\Delta\tilde{\gamma}_1)^2\right\} = E\{(\Delta i)^2 + \sin^2\tilde{\chi}(\Delta\varphi)^2\} \Big/ \tan^2\beta_S$$

$$= \left[\sigma_i^2 + 0.5\sigma_\varphi^2\right] \Big/ \tan^2\beta_S \tag{38}$$

Skew Slit Crossings

The sun sensor skew slit has a nominal inclination angle of i (which equals 28 deg for the sensor shown in Fig. 3) with respect to the sensor (X_{sb}, Y_{sb}) plane. The skew slit has the unit-normal vector $\boldsymbol{n}_2$ defined by

$$\boldsymbol{n}_2 = \cos i\, \boldsymbol{Y}_{\text{sb}} + \sin i\, \boldsymbol{Z}_{\text{sb}} \tag{39}$$

A necessary condition for the sun crossing the skew slit plane is $(\boldsymbol{n}_2 \cdot \boldsymbol{S}_{\text{sb}}) = 0$, which implies that the sun vector must be perpendicular to the skew slit normal at the crossing time. In the absence of biases, the ideal sun vector expression in Eq. (22) produces the following crossing angle:

$$\tilde{\gamma}_{2,\text{ideal}} = \arcsin(\tan i / \tan\beta_S) \tag{40}$$

This result is meaningful because crossings over the skew slit are not physically possible for a sun aspect angle β_S outside the interval $i < \beta_s < \pi$. Note that the sign of $\tilde{\gamma}_{2,\text{ideal}}$ is defined by the quadrant of the sun aspect angle.

When biases are present, the $\boldsymbol{S}_{\text{sb,pert}}$ term in Eq. (27) must be carried along, and the skew slit crossing condition $(\boldsymbol{n}_2 \cdot \boldsymbol{S}_{\text{sb}}) = 0$ leads to the following implicit equation for $\tilde{\gamma}_2$:

$$\tan\beta_S \sin\tilde{\gamma}_2 - \tan i = \Delta\varphi_i + \tan i \tan\beta_S(\Delta\varphi_i \sin\tilde{\gamma}_2 + \Delta\varphi_e \cos\tilde{\gamma}_2) \tag{41}$$

When introducing the expansion $\tilde{\gamma}_2 \cong \tilde{\gamma}_{2,\text{ideal}} + \Delta\tilde{\gamma}_2$ of the crossing angle in terms of the ideal crossing angle plus a small correction term, and substituting the result of Eq. (40), we find the small-angle result,

$$\Delta\tilde{\gamma}_2 \approx \Delta\varphi_e \tan i + \cos\beta_S \Delta\varphi_i / (S(\beta_S, i)\cos i) \tag{42}$$

The function $S(\beta_S, i)$ is an abbreviation for

$$S(\beta_s, i) = \sqrt{\sin^2\beta_S - \sin^2 i} \tag{43}$$

The square root is well defined for the physically meaningful interval of sun angles $i < \beta_S < \pi - i$.

The variance of $\Delta\tilde{\gamma}_2$ can be expressed in terms of the variances of the individual biases,

$$\sigma_2^2 = E\left\{(\Delta\tilde{\gamma}_2)^2\right\} = \left(\sigma_e^2 + 0.5\sigma_\varphi^2\right)\tan^2 i + \left(\sigma_i^2 + 0.5\sigma_\varphi^2\right)\cos^2\beta_S \Big/ \left(S^2(\beta_S, i)\cos^2 i\right) \quad (44)$$

Sun Aspect Angle Bias

The biases in the sun sensor's meridian and skew slit crossing times affect the calculation of the sun aspect angle. During in-flight operations, the sun aspect angle β_S is calculated from the difference between the crossing angles $\tilde{\gamma}_2$ and $\tilde{\gamma}_1$ as follows:

$$\beta_{S,\text{calc}} = \pi/2 - \arctan[\sin(\tilde{\gamma}_2 - \tilde{\gamma}_1)/\tan i] \quad (45)$$

After substituting the expansions for the slit crossing angles and the result (36), we find

$$\beta_{S,\text{calc}} \approx \pi/2 - \arctan[\sin(\tilde{\gamma}_{2,\text{ideal}} + \Delta\tilde{\gamma}_2 - \Delta\tilde{\gamma}_1)/\tan i] \quad (46)$$

The effect of the biases on the resulting sun aspect angle can be found by employing the expansion $\beta_{S,\text{calc}} = \beta_{S,\text{ideal}} + \Delta\beta_S$,

$$\Delta\beta_S \approx -[\sin\beta_S \cos\beta_S/\tan\tilde{\gamma}_{2,\text{ideal}}](\Delta\tilde{\gamma}_2 - \Delta\tilde{\gamma}_1)$$
$$= [S(\beta_S, i)\sin\beta_S/\cos i]\Delta\varphi_e + (\cos\beta_S/\sin i)[S(\beta_S, i) - \sin\beta_S/\cos i]\Delta\varphi_i \quad (47)$$

The variance of the bias error of the solar aspect angle σ_S^2 follows from the statistical properties of the input biases,

$$\sigma_S^2 = E\left\{(\Delta\beta_S)^2\right\} = \left(\sigma_e^2 + 0.5\sigma_\varphi^2\right)[S(\beta_S, i)\sin\beta_S/\cos i]^2 + \left(\sigma_i^2 + 0.5\sigma_\varphi^2\right)(\cos\beta_S/\sin i)^2[S(\beta_S, i) - \sin\beta_S/\cos i]^2 \quad (48)$$

C. Earth Sensor Measurements

The Earth sensor usually has two pencil beams with different pointing directions μ_1 and μ_2. For illustration, we consider only one pencil beam here. (Additional pencil beams can be treated in the same manner.) The pencil-beam pointing direction $\boldsymbol{p}$ with (generic) mounting angle μ (Fig. 5) has the following components in the (X_{sb}, Z_{sb}) plane:

$$\boldsymbol{p} = \sin\mu\boldsymbol{X}_{\text{sb}} + \cos\mu\boldsymbol{Z}_{\text{sb}} \quad (49)$$

We assume that the Earth's infrared radius R_{ir} is perfectly spherical with an instantaneous apparent radius ρ seen by the sensor from the spacecraft's orbital position $r = r(t)$,

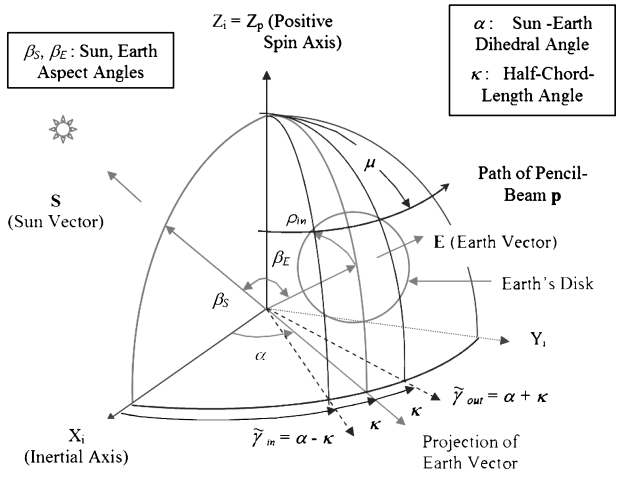

Fig. 5 Geometrical conditions of Earth sensor pencil-beam crossings.

$$\rho(r) = \arcsin(R_{\text{ir}}/r) \quad (50)$$

The Earth-in and Earth-out crossing conditions of the pencil beam follow from the fact that the angle between the pencil-beam pointing direction and the Earth vector must be equal to the apparent Earth's infrared radius,

$$\boldsymbol{E}\cdot\boldsymbol{p}_{\text{in}} = \cos\rho_{\text{in}}, \qquad \boldsymbol{E}\cdot\boldsymbol{p}_{\text{out}} = \cos\rho_{\text{out}} \quad (51)$$

The Earth vector $\boldsymbol{E}$ may be taken identical in these two expressions because the time difference is only a fraction of a spin period. The apparent Earth radii ρ_{in} and ρ_{out} refer to different locations on the Earth's infrared horizon so they may contain bias errors $\Delta\rho_{\text{in}}$ and $\Delta\rho_{\text{out}}$ that could differ significantly (by up to a few tenths of a degree).

Ideal Pencil-Beam Crossings

When substituting the pencil-beam pointing directions in Eq. (49) and the ideal Earth vector $\boldsymbol{E}_{\text{sb,ideal}}$ of Eq. (33a), we find the following results from the in- and out-crossing conditions in Eqs. (51):

$$\cos(\tilde{\gamma}_{\text{in,ideal}} - \alpha)\sin\beta_E \sin\mu + \cos\beta_E\cos\mu = \cos\rho_{\text{in}} \quad (52a)$$

$$\cos(\tilde{\gamma}_{\text{out,ideal}} - \alpha)\sin\beta_E \sin\mu + \cos\beta_E\cos\mu = \cos\rho_{\text{out}} \quad (52b)$$

Figure 5 shows that the expressions in the brackets represent the actual half-chord angles $-\kappa$ and $+\kappa$, respectively, that is, $\tilde{\gamma}_{\text{in,ideal}} = \alpha - \kappa$ and $\tilde{\gamma}_{\text{out,ideal}} = \alpha + \kappa$ with α the actual sun–Earth dihedral angle.

Earth Crossing Biases

In the presence of biases the Earth vector within the sensor frame will be perturbed as formulated by the result for $\boldsymbol{E}_{\text{sb,pert}}$ in Eq. (33b). The in and out crossing angles are now expanded as follows:

$$\tilde{\gamma}_{\text{in}} = \tilde{\gamma}_{\text{in,ideal}} + \Delta\tilde{\gamma}_{\text{in}}, \qquad \tilde{\gamma}_{\text{out}} = \tilde{\gamma}_{\text{out,ideal}} + \Delta\tilde{\gamma}_{\text{out}} \quad (53)$$

After substituting these expressions into Eq. (52) and expanding for small angles, we find

$$\Delta\tilde{\gamma}_{\text{in}} \approx -(\boldsymbol{E}_{\text{sb,pert}}\cdot\boldsymbol{p})/(\sin\kappa\sin\beta_E\sin\mu) = \Delta\varphi_i/\tan\mu + \Delta\varphi_e\{1/(\sin\kappa\tan\beta_E) - 1/(\tan\kappa\tan\mu)\} \quad (54a)$$

$$\Delta\tilde{\gamma}_{\text{out}} \approx (\boldsymbol{E}_{\text{sb,pert}}\cdot\boldsymbol{p})/(\sin\kappa\sin\beta_E\sin\mu) = \Delta\varphi_i/\tan\mu - \Delta\varphi_e\{1/(\sin\kappa\tan\beta_E) - 1/(\tan\kappa\tan\mu)\} \quad (54b)$$

These results have singularities when κ vanishes corresponding to the start and end of sensor coverage when the crossing sensitivities to biases are extreme. This issue has no consequences because these regions should not anyway be used for fine attitude determination purposes.[3]

Infrared Radii Biases

The biases $\Delta\rho_{\text{in}}$ and $\Delta\rho_{\text{out}}$ describe the biases in the apparent radii of the Earth's infrared disk at the location of the pencil-beam crossings. The expressions given in Eq. (53) are substituted in Eqs. (52). This leads to the following first-order shifts in the pencil-beam crossing angles induced by biases in the Earth's infrared horizon:

$$\Delta\tilde{\gamma}_{\text{in}} \approx -\Delta\rho_{\text{in}}\sin\rho/(\sin\kappa\sin\beta_E\sin\mu) \quad (55a)$$

$$\Delta\tilde{\gamma}_{\text{out}} \approx \Delta\rho_{\text{out}}\sin\rho/(\sin\kappa\sin\beta_E\sin\mu) \quad (55b)$$

Half-Chord-Length Biases

During flight operations, the half-chord-angle angle κ is calculated from the measured in and out crossing angles (Table 1 and Fig. 5),

$$\kappa_{\text{calc}} = \tfrac{1}{2}(\tilde{\gamma}_{\text{out}} - \tilde{\gamma}_{\text{in}}) \quad (56)$$

In fact, the measurements $\tilde{\gamma}_{\text{in}}$ and $\tilde{\gamma}_{\text{out}}$ are referenced to the time of the sun sensor meridian slit crossing, which may be affected by the bias error $\Delta\tilde{\gamma}_1$ given in Eq. (37). However, the latter bias acts in exactly the same manner for the in and out crossing angles so that

its effect on the calculation of κ_{calc} cancels. Equations (54) and (55) produce now the resulting $\Delta\kappa$ bias,

$$\Delta\kappa = \tfrac{1}{2}(\Delta\tilde{\gamma}_{\text{out}} - \Delta\tilde{\gamma}_{\text{in}}) = \Delta\varphi_e[1/\tan\kappa\tan\mu) - 1/\sin\kappa\tan\beta_E)] + \tfrac{1}{2}(\Delta\rho_{\text{in}} + \Delta\rho_{\text{out}})\sin\rho/(\sin\kappa\sin\beta_E\sin\mu) \quad (57)$$

Thus, the $\Delta\varphi_i$ bias has no effect on the chord-length calculation, but a uniform error in the Earth's infrared horizon definitely has an effect.[3,8]

Sun–Earth Azimuth Angle Calculation

The angle $\tilde{\gamma}_c$ designates the mean value of the $\tilde{\gamma}_{\text{in}}$ and $\tilde{\gamma}_{\text{out}}$ crossing angles and corresponds to the rotation angle at the time when the center of the Earth's disk coincides with the plane containing the pencil beam and the spin axis (Fig. 5). This instant is known as the chord-center crossing time and the angle $\tilde{\gamma}_c$ represents the attitude state variable α, that is, the sun–Earth dihedral angle in Figs. 1 and 5. During flight operations, the angle α is calculated from the individual in and out crossing angle measurements as follows:

$$\alpha_{\text{calc}} = \tilde{\gamma}_c = \tfrac{1}{2}(\tilde{\gamma}_{\text{in}} + \tilde{\gamma}_{\text{out}}) \quad (58)$$

In the absence of biases, the chord-center crossing angle α_{calc} would be equal to $\tilde{\gamma}_{c,\text{ideal}} = \frac{1}{2}(\tilde{\gamma}_{\text{in,ideal}} + \tilde{\gamma}_{\text{out,ideal}})$.

When biases are present, we expand $\tilde{\gamma}_c = \tilde{\gamma}_{c,\text{ideal}} + \Delta\tilde{\gamma}_c$ and obtain the error $\Delta\alpha$ as the mean value of the errors in the individual in and out crossings given in Eqs. (54) and (55). However, the effect induced by the sun sensor meridian slit crossing bias $\Delta\tilde{\gamma}_1 = \Delta\tilde{i}/\tan\beta_S$ established in Eq. (37) must be taken into account as well so that

$$\Delta\alpha = \tfrac{1}{2}(\Delta\tilde{\gamma}_{\text{in}} + \Delta\tilde{\gamma}_{\text{out}}) - \Delta\tilde{\gamma}_1 = \Delta\varphi_i(1/\tan\mu - 1/\tan\beta_S) + \tfrac{1}{2}(\Delta\rho_{\text{out}} - \Delta\rho_{\text{in}})\sin\rho/(\sin\kappa\sin\beta_E\sin\mu) \quad (59)$$

Thus, the bias $\Delta\varphi_e$ has no effect on the calculation of the sun–Earth dihedral angle. In the case when the pencil-beam mounting angle equals the sun aspect angle, the bias $\Delta\varphi_i$ will also be ineffective. The term containing the Earth's infrared biases vanishes when the biases $\Delta\rho_{\text{in}}$ and $\Delta\rho_{\text{out}}$ are taken equal, for example, when the bias in the Earth's infrared radius would be uniform.

IV. Propagation of Biases into Attitude Vector

We first summarize the propagation of the input biases (induced by the dynamic imbalance, sensor misalignments, and Earth radius errors) into the corresponding measurement angles. Subsequently, the propagation of the biases will be extended to errors in the resulting attitude solution. In practical applications, the magnitude of the Δe, Δi, and $\Delta\varphi$ biases would be specified in the form of a (Gaussian) probability density distribution with zero mean values and prescribed worst-case (3-σ) deviations. The present section will also address the propagation of the variances of the specified input biases into the corresponding variances of the attitude vector.

A. Biases in Measurement Angles

The generalized biases $\Delta\varphi_e$ and $\Delta\varphi_i$ are defined by the angle $\tilde{\chi}$ and the fundamental bias angles Δe, Δi, and $\Delta\varphi$ [Eqs. (28) and (29)]:

$$\begin{pmatrix}\Delta\varphi_e\\ \Delta\varphi_i\end{pmatrix} = \begin{bmatrix}\cos\tilde{\chi} & -1 & 0\\ \sin\tilde{\chi} & 0 & 1\end{bmatrix}\begin{pmatrix}\Delta\varphi\\ \Delta e\\ \Delta i\end{pmatrix} \quad (60)$$

The fundamental biases $\Delta\varphi$, Δe, and Δi are obviously independent and may be assumed to be normally distributed with zero-mean value. The angle $\tilde{\chi}$ on the other hand is uniformly distributed. The covariance terms of the derived biases $\Delta\varphi_e$ and $\Delta\varphi_i$ can be calculated as

$$\sigma_1^2 = E\{(\Delta\varphi_e)^2\} = \tfrac{1}{2}\sigma_\varphi^2 + \sigma_e^2 \quad (61a)$$

$$\sigma_2^2 = E\{(\Delta\varphi_i)^2\} = \tfrac{1}{2}\sigma_\varphi^2 + \sigma_i^2 \quad (61b)$$

By virtue of the adopted statistical characteristics of the biases $\Delta\varphi$, Δe, and Δi, it follows that $\Delta\varphi_e$ and $\Delta\varphi_i$ in Eq. (60) are uncorrelated so that $E\{(\Delta\varphi_e)(\Delta\varphi_i)\} = 0$.

For simplicity, we assume here that the crossing biases of the Earth's infrared disk are identical, that is, $\Delta\rho = \Delta\rho_{\text{in}} = \Delta\rho_{\text{out}}$. In practice, seasonal effects, that is, the north–south thermal gradient, may induce a sizeable difference in the biases $\Delta\rho_{\text{in}}$ and $\Delta\rho_{\text{out}}$. The effects of the biases on the measurement angles were established in Eqs. (47), (57), and (59) and are summarized as

$$\begin{pmatrix}\Delta\beta_S\\ \Delta\kappa\\ \Delta\alpha\end{pmatrix} = [B]\begin{pmatrix}\Delta\varphi_e\\ \Delta\varphi_i\\ \Delta\rho\end{pmatrix} \quad (62)$$

The matrix $[B]$ is defined as

$$[B] = \begin{bmatrix}b_{11} & b_{12} & 0\\ b_{21} & 0 & b_{23}\\ 0 & b_{32} & 0\end{bmatrix} \quad (63)$$

with nonzero terms

$$b_{11} = -\sin\beta_S S(\beta_S, i)/\cos i$$
$$b_{12} = (\cos\beta_S/\sin i)[S(\beta_S, i) - \sin\beta_S/\cos i]$$
$$b_{21} = 1/(\tan\kappa\tan\mu) - 1/(\sin\kappa\tan\beta_E)$$
$$b_{23} = \sin\rho/(\sin\kappa\sin\beta_E\sin\mu)$$
$$b_{32} = (1/\tan\mu - 1/\tan\beta_S) \quad (64)$$

Note that the b_{33} term has vanished because of the assumption that $\Delta\rho_{\text{out}}$ equals $\Delta\rho_{\text{in}}$.

The propagation of the covariances σ_1^2, σ_2^2, and σ_3^2, which are associated with the independent input biases $\Delta\varphi_e$, $\Delta\varphi_i$, and $\Delta\rho$, into those of the measurement angles $\Delta\beta_S$, $\Delta\kappa$, and $\Delta\alpha$ follows from Eq. (62),

$$[C] = [B]\begin{bmatrix}\sigma_1^2 & 0 & 0\\ 0 & \sigma_2^2 & 0\\ 0 & 0 & \sigma_3^2\end{bmatrix}[B]^T = \begin{bmatrix}\sigma_S^2 & \sigma_{S\kappa} & \sigma_{S\alpha}\\ \sigma_{S\kappa} & \sigma_\kappa^2 & 0\\ \sigma_{S\alpha} & 0 & \sigma_\alpha^2\end{bmatrix} \quad (65)$$

The nonzero entries of $[C]$ are

$$\sigma_S^2 = b_{11}^2\sigma_1^2 + b_{12}^2\sigma_2^2, \qquad \sigma_\kappa^2 = b_{21}^2\sigma_1^2 + b_{23}^2\sigma_3^2$$
$$\sigma_\alpha^2 = b_{32}^2\sigma_2^2, \qquad \sigma_{S\kappa} = b_{11}b_{21}\sigma_1^2, \quad \sigma_{S\alpha} = b_{12}b_{32}\sigma_2^2 \quad (66)$$

B. Earth Aspect Angle Calculation

The bias in the Earth aspect angle $\Delta\beta_E$ can in principle be calculated from the bias $\Delta\kappa$ in the measured half-chord angle using the more conventional form of Eqs. (52). In typical applications,[3] there will be two pencil beams (with different mounting angles μ_i, $i = 1, 2$) that have simultaneous coverage during the attitude-determination interval. A minimum-variance solution of the Earth aspect angle can be established by means of a linear combination of the half-cord angles κ_i, $i = 1, 2$, measured by the two pencil beams. This involves the linearizations of Eqs. (52) and the introduction of weights defined by the respective sensitivity coefficients $f_i = \partial\beta_E/\partial\kappa_i$ of each pencil beam during the relevant interval,

$$f_i = \sin\beta_E\sin\mu_i\sin\kappa_i/(\cos\beta_E\sin\mu_i\cos\kappa_i - \sin\beta_E\cos\mu_i) \quad (i = 1, 2) \quad (67)$$

In a similar way as in Eq. (6) of Ref. 3, we can express the bias $\Delta\beta_E$ in terms of the measurement biases $\Delta\kappa_i$ of each of the two pencil beams,

$$\Delta\beta_E = g_1\Delta\kappa_1 + g_2\Delta\kappa_2 \quad (68)$$

with

$$g_i = (1/f_i)\Big/\left(1\Big/f_1^2 + 1\Big/f_2^2\right) \qquad (i = 1, 2) \tag{69}$$

The two pencil beams also produce the two dihedral measurements α_i, $i = 1, 2$. Their biases should be combined into the resulting $\Delta\alpha$ bias using equal weights, that is, $\Delta\alpha = \frac{1}{2}(\Delta\alpha_1 + \Delta\alpha_2)$.

We can now modify Eqs. (62) and (63) as follows:

$$\begin{pmatrix} \Delta\beta_S \\ \Delta\beta_E \\ \Delta\alpha \end{pmatrix} = [\tilde{B}] \begin{pmatrix} \Delta\varphi_e \\ \Delta\varphi_i \\ \Delta\rho \end{pmatrix} = \begin{bmatrix} b_{11} & b_{12} & 0 \\ \tilde{b}_{21} & 0 & \tilde{b}_{23} \\ 0 & \tilde{b}_{32} & 0 \end{bmatrix} \begin{pmatrix} \Delta\varphi_e \\ \Delta\varphi_i \\ \Delta\rho \end{pmatrix} \tag{70}$$

The following matrix coefficients are modified relative to Eqs. (64):

$$\tilde{b}_{21} = g_1[1/(\tan\kappa_1 \tan\mu_1) - 1/(\sin\kappa_1 \tan\beta_E)] + g_2[1/(\tan\kappa_2 \tan\mu_2) - 1/(\sin\kappa_2 \tan\beta_E)]$$

$$\tilde{b}_{23} = g_1 \sin\rho_1/(\sin\kappa_1 \sin\beta_E \sin\mu_1) + g_2 \sin\rho_2/(\sin\kappa_2 \sin\beta_E \sin\mu_2)$$

$$\tilde{b}_{32} = \tfrac{1}{2}(1/\tan\mu_1 + 1/\tan\mu_2) - 1/\tan\beta_S \tag{71}$$

The covariance matrix in Eq. (65) must now be modified into

$$[\tilde{C}] = [\tilde{B}] \begin{bmatrix} \sigma_1^2 & 0 & 0 \\ 0 & \sigma_2^2 & 0 \\ 0 & 0 & \sigma_3^2 \end{bmatrix} \qquad [\tilde{B}]^T = \begin{bmatrix} \sigma_S^2 & \sigma_{SE} & \sigma_{SN} \\ \sigma_{SE} & \sigma_E^2 & 0 \\ \sigma_{SN} & 0 & \sigma_N^2 \end{bmatrix} \tag{72}$$

with the following updated entries compared to Eqs. (66):

$$\sigma_E^2 = \tilde{b}_{21}^2\sigma_1^2 + \tilde{b}_{23}^2\sigma_3^2, \qquad \sigma_{SE} = b_{11}\tilde{b}_{21}\sigma_1^2$$
$$\sigma_N^2 = \tilde{b}_{32}^2\sigma_2^2, \qquad \sigma_{SN} = b_{12}\tilde{b}_{32}\sigma_2^2 \tag{73}$$

C. Attitude Determination Bias

Subsequently, we analyze the effects of the measurement biases on the attitude solution in a single-frame attitude determination procedure. The equations expressing the spin axis attitude $\boldsymbol{Z}_p$ in terms of the angles β_S, β_E, and α may be written as [Ref. 3, Eqs. (3)]

$$\boldsymbol{S} \cdot \boldsymbol{Z}_p = \cos\beta_S, \qquad \boldsymbol{E} \cdot \boldsymbol{Z}_p = \cos\beta_E$$
$$(\boldsymbol{S} \times \boldsymbol{E}) \cdot \boldsymbol{Z}_p = \sin\beta_S \sin\beta_E \sin\alpha \tag{74}$$

It is most convenient to refer the single-frame attitude solution to the quasi-inertial sun–Earth frame that is based on the instantaneous sun and Earth vectors (Fig. 6). The X axis is along the sun vector $\boldsymbol{S}$, the Y axis is within the plane formed by the sun and Earth vectors along the unit vector $\boldsymbol{T} = (\boldsymbol{E} - \cos\psi\boldsymbol{S})/\sin\psi$, and the third axis is along the normal to the sun–Earth plane, $\boldsymbol{N} = (\boldsymbol{S} \times \boldsymbol{E})/\sin\psi$. These three axes form an orthogonal triad that can easily be transformed to the geocentric J2000 reference frame by using the components of the vectors $\boldsymbol{S}$ and $\boldsymbol{E}$.

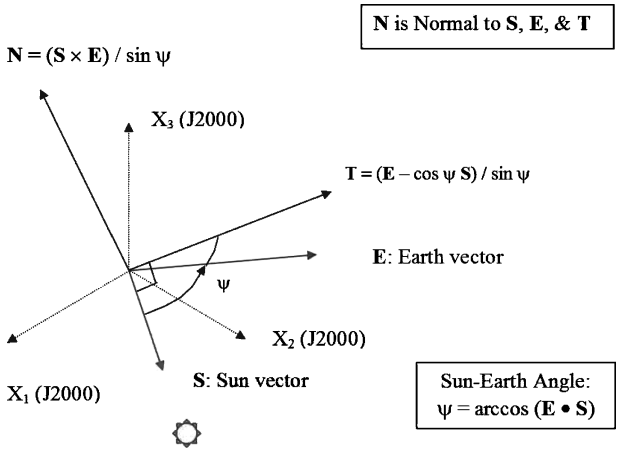

Fig. 6 Sun–Earth frame defined by sun and Earth unit vectors.

The measurement equations (74) may be written in the matrix form

$$\boldsymbol{y} = [H]\boldsymbol{Z}_p \tag{75}$$

The measurement vector $\boldsymbol{y}$ and the measurement matrix $[H]$ are defined as

$$\boldsymbol{y} = (\cos\beta_S, \cos\beta_E, \sin\beta_S \sin\beta_E \sin\alpha/\sin\psi)^T \tag{76}$$

$$[H] = \begin{bmatrix} 1 & 0 & 0 \\ \cos\psi & \sin\psi & 0 \\ 0 & 0 & 1 \end{bmatrix} \tag{77}$$

Provided that the sun and Earth vectors are not collinear, that is, $\psi \neq 0$ and $\psi \neq 180$ deg, the matrix $[H]$ can be inverted and the single-frame attitude solution follows as

$$\boldsymbol{Z}_p = [H]^{-1}\boldsymbol{y} \tag{78}$$

with

$$[H]^{-1} = \left(\frac{1}{\sin\psi}\right) \begin{bmatrix} \sin\psi & 0 & 0 \\ -\cos\psi & 1 & 0 \\ 0 & 0 & \sin\psi \end{bmatrix} \tag{79}$$

The following explicit components of the determined attitude vector in the sun–Earth frame can now be calculated:

$$\boldsymbol{Z}_p = (\cos\beta_S \sin\psi, \cos\beta_E - \cos\psi\cos\beta_S, \sin\beta_S \sin\beta_E \sin\alpha)^T/\sin\psi \tag{80}$$

In the presence of the biases $\Delta\beta_S$, $\Delta\beta_E$, and $\Delta\alpha$, we would obtain a slightly different perturbed attitude solution $\boldsymbol{Z}_{p,\text{pert}}$. An explicit result for the error $\Delta\boldsymbol{Z}_p = \boldsymbol{Z}_{p,\text{pert}} - \boldsymbol{Z}_p$ in the determined attitude can be constructed by means of a small-angle expansion of Eq. (80) in terms of $\Delta\beta_S$, $\Delta\beta_E$, and $\Delta\alpha$,

$$\Delta\boldsymbol{Z}_p \approx [A](\Delta\beta_S, \Delta\beta_E, \Delta\alpha)^T \tag{81}$$

with

$$[A] = \left(\frac{1}{\sin\psi}\right) \begin{bmatrix} -\sin\psi\sin\beta_S & 0 & 0 \\ \cos\psi\sin\beta_S & -\sin\beta_E & 0 \\ \cos\beta_S\sin\beta_E\sin\alpha & \sin\beta_S\cos\beta_E\sin\alpha & \sin\beta_S\sin\beta_E\cos\alpha \end{bmatrix} \tag{82}$$

It can be confirmed [with the help of Eq. (5)] that the vector $\boldsymbol{Z}_p$ in Eq. (80) satisfies the normality condition $|\boldsymbol{Z}_p| = 1$. However, the perturbed attitude solution $\boldsymbol{Z}_{p,\text{pert}}$ may violate the normality condition due to the bias effects and should be normalized. The attitude error δ_{att} is defined as the half-cone pointing angle deviation of the perturbed attitude vector $\boldsymbol{Z}_{p,\text{pert}}$ from the ideal attitude $\boldsymbol{Z}_p$. Because the biases are small, the geometrical result $\delta_{\text{att}} \approx |\Delta\boldsymbol{Z}_p|$ represents a valid useful approximation,

$$\delta_{\text{att}} \approx |\Delta\boldsymbol{Z}_p| = \left\{(\Delta\beta_S, \Delta\beta_E, \Delta\alpha)[A]^T[A](\Delta\beta_S, \Delta\beta_E, \Delta\alpha)^T\right\}^{\frac{1}{2}} \tag{83}$$

After writing the elements of the matrix $[A]$ in Eq. (82) as a_{jk}, $j, k = 1, 2, 3$, we may express the variance of the attitude error in terms of the variances defined in Eqs. (66) and (73),

$$\sigma_{\text{att}}^2 = E\left\{\delta_{\text{att}}^2\right\} = \left(a_{11}^2 + a_{21}^2 + a_{31}^2\right)\sigma_S^2 + \left(a_{22}^2 + a_{32}^2\right)\sigma_E^2 + a_{33}^2\sigma_N^2 + 2(a_{21}a_{22} + a_{31}a_{32})\sigma_{SE} + 2a_{31}a_{33}\sigma_{SN} \tag{84}$$

Finally, the attitude error can be expressed explicitly in the variances of the fundamental biases σ_1^2, σ_2^2, and σ_3^2 with the help of the expressions in Eqs. (61), (64), (71), and (73). The variance in Eq. (84) is useful for performing an evaluation of the expected attitude error based on the known specifications of the input biases.

V. Procedures for Reconstruction of Biases

The present model offers practical methods for reconstructing the input biases on the basis of their signatures in the measurement residuals. (These residuals denote the differences between the actually realized measurements and the predicted measurements obtained from a high-fidelity simulator using the determined attitude as input.) The result in Eq. (70) may be interpreted in the sense that each of the biases $\Delta\varphi_e$, $\Delta\varphi_i$, and $\Delta\rho$ induces effects on the angular measurements that may actually be observable in the residuals $(\Delta\beta_S)_{\text{res}}$, $(\Delta\beta_E)_{\text{res}}$, and $(\Delta\alpha)_{\text{res}}$. Equation (70) may then be inverted to calculate the input biases from the observed measurement residuals. As an alternative procedure, the system in Eq. (62) may be used because the residual $(\Delta\kappa_E)_{\text{res}}$ represents a more direct measurement.

For illustration, we consider the case where there is only one pencil beam and the Earth's in and out crossing biases are assumed to be identical. Equation (70) shows that all of the three biases can be calculated successively from the measurement residuals as follows:

$$\Delta\varphi_{i,\text{calc}} = (\Delta\alpha)_{\text{res}}/\tilde{b}_{32}, \quad \Delta\varphi_{e,\text{calc}} = [(\Delta\beta_S)_{\text{res}} - b_{12}\Delta\varphi_{i,\text{calc}}]/b_{11}$$

$$\Delta\rho_{\text{calc}} = [(\Delta\beta_E)_{\text{res}} - \tilde{b}_{21}\Delta\varphi_{e,\text{calc}}]/\tilde{b}_{23} \tag{85}$$

The residuals may be averaged over a relatively short interval (up to 30 min) over which they (as well as the functions $\tilde{b}_{jk}$) remain sufficiently steady.

When different biases are acting for the in and out crossings of the Earth infrared disk (for instance, due to the north–south effect) the results in Eq. (85) are not valid. Therefore, we consider now a situation where the biases $\Delta\rho_{\text{in}}$ and $\Delta\rho_{\text{out}}$ are different (and we use two pencil beams as well). The measurement relations in Eqs. (47), (57), and (59) produce now five equations with six unknowns and so unambiguous solutions can unfortunately not be constructed. However, in the special case when $\Delta\varphi_e$ and $\Delta\varphi_i$ can be neglected relative to $\Delta\rho_{\text{in}}$ and $\Delta\rho_{\text{out}}$, the applicable in and out crossing biases can be reconstructed for each of the two pencil beams $i = 1, 2$ as follows:

$$\Delta\rho_{\text{in},i} \approx [(\Delta\kappa_i)_{\text{res}} - (\Delta\alpha_i)_{\text{res}}]/b_{23,i}$$

$$\Delta\rho_{\text{out},i} \approx [(\Delta\kappa_i)_{\text{res}} + (\Delta\alpha_i)_{\text{res}}]/b_{23,i} \tag{86}$$

Afterwards, the hypothesis that $\Delta\varphi_e$ and $\Delta\varphi_i$ were indeed negligible should be verified.

VI. Discussion of Results

The preceding results have been applied to the specific conditions of the CONTOUR spacecraft that was launched into a highly elliptical phasing orbit on 3 July 2002. The Earth sensor coverage intervals occurred after apogee at an altitude range between about 70,000 and 35,000 km with Earth aspect angles decreasing from about 70 to 50 deg (van der Ha et al.[3]).

A. Sun Aspect Angle Error

The calculation of the sun aspect angle can be adversely affected by the biases Δe, Δi, and $\Delta\varphi$ [Eq. (47)]. Figure 7 shows the sensitivities $\partial\beta_S/\partial e$ and $\partial\beta_S/\partial i$ of the calculated sun angle to elevation and inclination biases as a function of the solar aspect angle. Four additional results for the sensitivity $\partial\beta_S/\partial\varphi$ of the sun angle to tilt biases with $\tilde{\chi} = 45$, 135, 225, and 315 deg [Eqs. (29)] are shown in Fig. 7. It is seen that the resulting error in the calculated sun angle is at most equal to the relevant input bias itself.

B. Earth Aspect Angle Error

Figure 8 shows the effect of an elevation angle bias on the Earth sensor half-chord measurements, as well as on the resulting Earth aspect angle. The Earth aspect angle is obtained from two chord-angle measurements using the method outlined in Eqs. (67–69). This approach benefits the Earth aspect angle sensitivity $\partial\beta_E/\partial\tilde{e}$ when both pencil beams have simultaneous coverage. The error in the Earth aspect angle over this interval is at most slightly larger than the elevation bias even though the errors in the measured half-chord angles vary widely.

Figure 9 shows the sensitivities of the Earth sensor measurements to biases in the infrared Earth radius. We find that the Earth aspect angle sensitivity $\partial\beta_E/\partial\rho$ remains within the bounds -1.25 and $+1.35$ over the combined pencil-beam coverage interval. Note that the bias error $\Delta\beta_E$ vanishes at about 37.1 h. This is because the two half-cord measurements have equal but opposite weights at this time so the combined solution for the Earth aspect angle becomes exact. (Note that the present results are based on equal biases in the Earth infrared radii.)

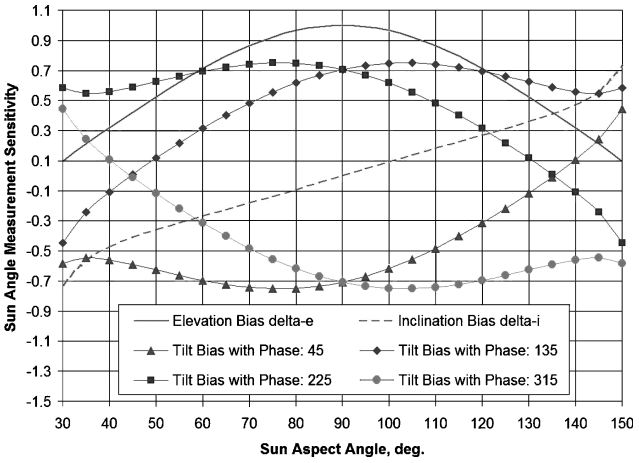

Fig. 7 Sun angle sensitivity to elevation, inclination, and tilt biases.

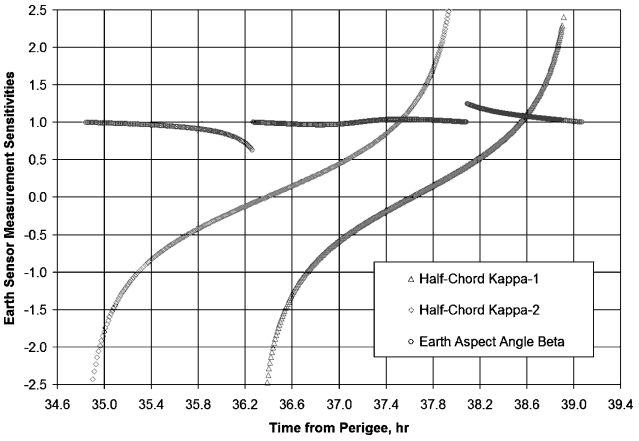

Fig. 8 Earth sensor measurement sensitivities to elevation bias.

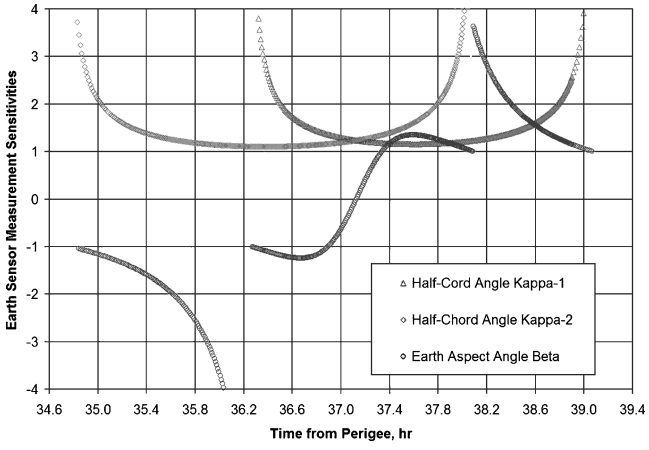

Fig. 9 Earth sensor measurement sensitivities to Earth radius bias.

Table 2 Reconstruction of biases in the Earth radii

Half chords,[a] deg		Chord centers,[a] deg		Earth Radii[b]			
$(\Delta\kappa_1)_{res}$	$(\Delta\kappa_2)_{res}$	$(\Delta\alpha_1)_{res}$	$(\Delta\alpha_2)_{res}$	$\Delta\rho_{in,1}$	$\Delta\rho_{in,2}$	$\Delta\rho_{out,1}$	$\Delta\rho_{out,2}$
−0.22	−0.12	0.03	−0.13	−0.20	0.01	−0.16	−0.19
After corrections for all four biases in Earth radii							
0	0	0.07	−0.07	−0.06	0.06	0.06	−0.06

[a]Observed residuals. [b]Reconstructed Biases.

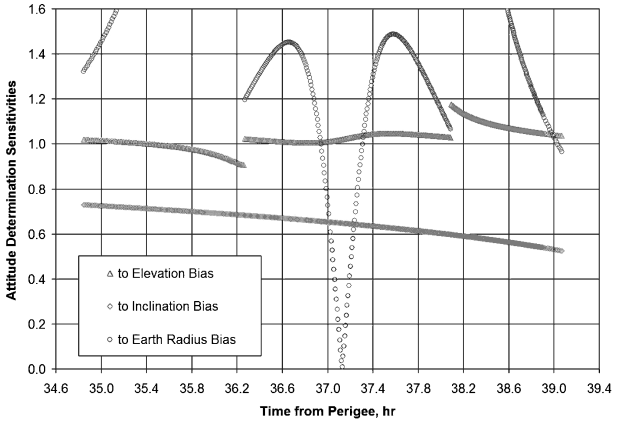

Fig. 10 Attitude error sensitivities to elevation, inclination, and Earth radius biases.

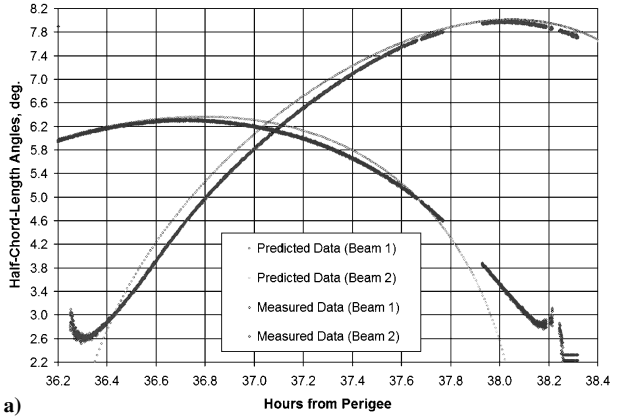

a)

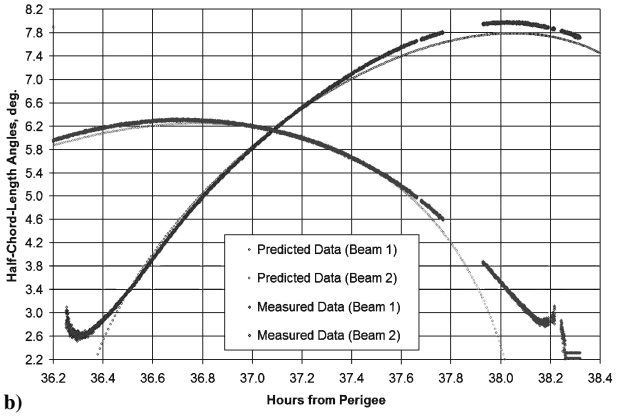

b)

Fig. 11 Half chord residuals a) before and b) after correction of Earth radii biases.

C. Attitude Determination Error

Figure 10 shows the sensitivities of the half-cone pointing error of the single-frame attitude solution relative to the three input biases [Eqs. (81) and (82)]. The variations over time are caused by the underlying geometry in terms of Earth aspect angle. It can be concluded that the resulting sensitivities of the attitude error over the combined sensor coverage interval are limited by 1.05, 0.7, and 1.5, respectively.

D. Results of Bias Reconstructions

Table 2 shows the results of the reconstruction of the Earth radius biases by the model of Eqs. (86). There appears to be a systematic elevation error Δe of about −0.06 deg (which exhibits itself also in the residual of the sun aspect angle) and so we can not reduce the biases further than shown here using the model of Eqs. (86).

Figure 11a shows the residuals during the prime attitude determination interval between 36.9 and 37.4 h (CONTOUR, 13 August 2002). Figure 11b shows the significant reduction of the chord-angle residuals after correcting for the reconstructed biases.

VII. Conclusions

A practical model is presented for describing the effects of biases induced during spacecraft design, for example, dynamic imbalance and sensor-mounting alignment errors, and by variations in the infrared Earth radius observed by the Earth sensor. The measurement equations for the sun sensor meridian and skew slit crossings and for the Earth sensor's pencil-beams in and out crossings of the Earth's infrared disk are established. A first-order perturbation technique is used for obtaining the angular measurements in the presence of the relevant biases. The propagation of the biases into the resulting attitude solution is established through a realistic single-frame attitude-determination procedure. The results are useful for predicting the attitude-determination error on the basis of the input biases. Furthermore, if statistical information on the expected biases is available, similar statistical properties may be calculated for the expected attitude error. Finally, a few practical procedures for the reconstruction of the biases from the observed measurement residuals are presented. The results have been applied to the conditions of the CONTOUR spacecraft during its phasing orbits in August 2002. In particular, the sensitivities of the sun and Earth sensor measurements, as well as the attitude to the relevant biases are illustrated and the reconstruction of the individual infrared Earth radius biases is demonstrated.

References

[1]Farquhar, R. W., and Dunham, D., "The Indirect Launch Mode: A New Launch Technique for Interplanetary Missions," *Acta Astronautica*, Vol. 45, No. 4–9, 1999, pp. 491–497.

[2]van der Ha, J. C., "Attitude Determination Covariance Analysis for Geostationary Transfer Orbits," *Journal of Guidance, Control, and Dynamics*, Vol. 9, No. 2, 1986, pp. 156–163.

[3]van der Ha, J., Rogers, G., Dellinger, W., and Stratton, J., "CONTOUR Phasing Orbits: Attitude Determination & Control Concepts and Flight Results," *AAS Advances in the Astronautical Sciences*, edited by D. J. Scheeres, M. E. Pittelkau, R. J. Proulx, and L. A. Cangahuala, Vol. 114, Part 3, Univelt, Inc., San Diego, CA, 2003, pp. 767–781; also American Astronautical Society, Paper AAS-03-150, Feb. 2003.

[4]Wertz, J. R. (ed.), *Spacecraft Attitude Determination and Control*, Reidel, Dordrecht, The Netherlands, 1978.

[5]Fraiture, L., "Spin-Axis Attitude Determination by a Controlled Correlation Method," *Journal of Spacecraft and Rockets*, Vol. 42, No. 1, 2005, pp. 58–65.

[6]Palimaka, J. J., Grisé, A. J., Burlton, B. V., and Overduin, J. M., "Elimination of Attitude Determination Error Constraints in Launch Windows for Geosynchronous Missions," *AAS Advances in Astronautical Sciences*, edited by C. L. Thornton, R. J. Proulx, J. E. Prussing, and F. Hoots, Vol. 71, Univelt, Inc., San Diego, CA, 1989, pp. 261–272.

[7]Sullivan, W. I., Paluszek, M. A., and Surka, D. M., "The Spin Axis Attitude Determination Package," *AAS Advances in Astronautical Sciences*, edited by R. H. Bishop, R. D. Culp, D. L. Mackison, and M. Evans, Univelt, Inc., San Diego, CA, 1999, pp. 503–522.

[8]van der Ha, J. C., "Equal Chord Attitude Determination Method for Spinning Spacecraft," *Journal of Guidance, Control and Dynamics*, Vol. 28, No. 5, 2005, pp. 997–1005.